WELDING RESEARCH

SUPPLEMENT TO THE *WELDING JOURNAL*, MARCH 1987

Sponsored by the American Welding Society and the Welding Research Council

Readers are advised that all papers published in the *Welding Journal's* Research Supplement undergo Peer Review before publication for: 1) originality of the contribution; 2) technical value to the welding community; 3) prior publication of the material being reviewed; 4) proper credit to others working in the same area; and 5) justification of the conclusions based on the results.

The names of the more than 160 individuals serving on the AWS Peer Review Panel are published periodically. All are experts in their respective technical areas, and all are volunteers in the program.

Sulfide Stress Corrosion Cracking in Low-Alloy Steel Inertia Friction Welds

Banding and transversely oriented elongated sulfide inclusions at the weld interfaces make the low-alloy steel friction welds susceptible to cracking

BY M. D. TUMULURU

ABSTRACT. Sulfide stress corrosion (SSC) cracking behavior of quenched and tempered low-alloy steel inertia friction welds was studied using the NACE test on smooth tensile specimens. Inertia friction welds were made between AISI 4137-H steel and Grade E pipe (per API specification 5A). The welds were quenched and tempered to a hardness of 33 HRC. The SSC cracking resistance of quenched and tempered AISI 4137-H steel in the transverse direction (with respect to metalworking direction) was also studied at a hardness of 33 HRC. Time to failure versus loading (applied) stress plots were made for both the welds and AISI 4137-H steel. Scanning electron microscope (SEM) and optical metallographic techniques were utilized to study the fracture and crack morphologies in the test specimens.

The study showed that the AISI 4137-H steel had higher susceptibility to SSC cracking in the transverse direction than in the longitudinal direction. The reason for this was attributed to the presence of elongated sulfide inclusions perpendicular to the loading axis. Banding at the weld interfaces caused during the inertia friction welding was found to be the reason the welds exhibited the highest degree of susceptibility to SSC cracking. The use of the interrupted SSC tests made it possible to observe clearly the hydrogen fracture morphologies in the specimens.

M. D. TUMULURU is a Research Metallurgist at Spang and Co., Butler, Pa.

KEY WORDS
Sulfide Corrosion
Corrosion Cracking
Stress Corrosion
Friction Weld Cracks
Sulfide SC Cracking
Sulfide Inclusions
Hydrogen Fracture
NACE Test
Low Alloy Steels
Tool Joints and Pipe

Introduction

Cracking of high-strength low-alloy steels due to hydrogen sulfide (H_2S) is a form of hydrogen embrittlement. The hydrogen sulfide reacts with the steel, forming FeS and atomic hydrogen, some of which will enter the steel and cause brittle failure (Ref. 1). Recently, it was shown that hydrogen is the causal factor in the SSC cracking of low-alloy steels and that SSC is a manifestation of hydrogen embrittlement (Ref. 2). Among the various microstructures investigated, those consisting of relatively fine, spheroidized carbides uniformly distributed in ferrite were found to have the maximum resistance to SSC cracking (Ref. 3). Such microstructures can be typically produced from steels with fine prior austenite grain size, quenched to fully martensitic microstructure and then tempered at high temperatures.

The drill pipe used in oil drilling consists of a central tubular section, called the pipe, welded to couplings, called tool joints. The male coupling, called the pin, contains external threads, while the

Table 1—Chemical Compositions of the Steels Used in the Study

Steel	Element (wt-%)								
	C	Mn	Si	Ni	Mo	Cu	Cr	S	P
Steel A (tool joint)	0.38	0.82	0.23	0.08	0.19	0.12	0.93	0.022	0.008
Steel B (pipe)	0.43	1.72	0.22	<0.005	0.15	0.02	0.03	0.011	0.010

female coupling, called the box, has internal threads. Both the tool joints are generally made of quenched and tempered AISI 4137-H steel and can be welded to the pipe using the inertia friction welding process (Ref. 4).

The drill pipes quite often are exposed to hydrogen sulfide during drilling. The hydrogen sulfide can embrittle both the pipe and the tool joints. Sulfide stress corrosion cracking resistance of steels used in the tool joints and pipes has been widely studied (Refs. 5-9). However, very little information is available on the sulfide stress corrosion cracking behavior of low-alloy steel inertia friction welds.

It was shown earlier that due to the plastic flow that occurs at the weld interfaces during inertia friction welding, elongated nonmetallic inclusions become transversely oriented (with reference to the metalworking direction) at the weld interfaces (Refs. 4,10). The disadvantage of such a reorientation of inclusions along the transverse direction is that the toughness of the inertia friction welds is drastically reduced (Refs. 4,11). Therefore, the inertia friction welds may be more susceptible to sulfide stress corrosion cracking than either the tool joints or the pipes. The purpose of the present investigation was to study the sulfide stress corrosion (SSC) cracking behavior of low-alloy steel inertia friction welds in the quenched and tempered condition. SSC cracking resistance of AISI 4137-H steel in the transverse direction was also evaluated for comparison purposes.

Materials and Experimental Procedure

Inertia friction welds were made between dissimilar steels—Steel A (AISI 4137-H) and Steel B. Steel B corresponds to API Grade E pipe (per API specification 5A). The only API specification 5A chemical composition requirements for Grade E pipe are that the phosphorus and sulfur contents be limited to 0.040% and 0.060% maximum each, respectively.

The tool joints (end couplings) made of Steel A were used in the quenched and tempered condition, whereas the pipes made of Steel B were normalized and tempered prior to welding. The compositions of Steel A and Steel B used in making the test welds are listed in Table 1.

The mating faces of the tool joints and the pipes were machined flat to a surface roughness of approximately 1.6 μm to avoid any mismatch between the parts. In each case, the tool joint was clamped in a chuck, rotated to a predetermined speed, and the stationary pipe was brought into contact with the rotating coupling under an applied axial pressure to form the weld. Table 2 lists the welding conditions used in the study to make the test welds.

Longitudinal sections cut from the weld area were austenitized at 870°C (1598°F) for 15 min in a salt bath and oil quenched. They were then tempered at 685°C (1265°F) for 2 min and 20 s. The as-tempered hardness of the weld specimens on the tool joints (AISI 4137-H steel) was 33 HRC. A hardness of 33 HRC was chosen because much of the earlier work on this steel was done at this hardness level (Ref. 12). The weld sections were then machined to the required specimen dimensions.

To study the SSC cracking behavior of AISI 4137-H steel in the transverse direction, strips were cut from the original square billet stock in the transverse direction (with regard to the metalworking direction). The strips were first normalized at 900°C (1652°F) under nitrogen atmosphere for one hour, austenitized at 870°C (1598°F) for 15 min in a salt bath, and oil quenched. The specimens were then tempered at 685°C for 2 min and 20 s. The hardness of the as-tempered strips was 33 HRC. The strips were then machined to the required specimen dimensions. The mechanical properties of the welds, Steel B (pipe) and Steel A (AISI 4137-H steel in both longitudinal and transverse directions) in the quenched and tempered condition are listed in Table 3.

The SSC testing was conducted using NACE procedure on smooth tensile specimens (Ref. 13). The specimens in the test were held under an applied tensile load and exposed to a corrosive medium consisting of aqueous solution of 5 percent NaCl and 0.5 percent acetic acid. The corrosive medium, which was contained in an environmental chamber around the specimen, was saturated with hydrogen sulfide by constantly bubbling the gas into the corrosive medium for the duration of the test. The stress on the specimens was applied using a proof ring. The inertia friction weld specimens were machined in such a way that the weld centerline between Steel A and Steel B was at the center of the gage length in the SSC test specimens. The SSC test setup showing the test specimen, specimen chamber, and the proof ring is shown in Fig. 1.

The SSC test specimens from the welds were loaded from 103.4 MPa (15,000 psi) to 206.8 MPa (30,000 psi) at increments of 34.5 MPa (5000 psi) and from 206.8 MPa (30,000 psi) to 413.7 MPa (60,000 psi) at 68.9 MPa (10,000 psi) increments. The SSC test specimens machined along the transverse direction of AISI 4137-H steel were loaded from 137.8 MPa (20,000 psi) to 413.7 MPa (60,000 psi) at increments of 34.5 MPa (5000 psi). The time to failure was noted in each case. Plots were made between the loading stress (applied stress) and the time to failure for the welds and AISI 4137-H steel in the transverse direction.

Three SSC test specimens from the inertia friction welds were loaded in the test cell at 137.8 MPa (20,000 psi) for 4 h, unloaded, and pulled in a tensile testing

Table 2—Inertia Friction Welding Conditions

Moment of inertia (Kg · m^2)	87.0
Speed of rotation[a] (m/s)	8.3
Axial pressure (MPa)	22.1
Time to weld (s)	11.0
Energy input[b] (J/cm^2)	16,870

[a]Peripheral velocity.
[b]Total energy input to the weld per unit area.

Table 3—Mechanical Properties of the Steels and Welds in the Q & T Condition

Steel		Yield Strength (MPa)	Ultimate Tensile Strength (MPa)	Elongation (%)
Steel A (AISI 4137-H)	Longitudinal[a]	1020	1087	18.5
	Transverse[b]	988	1064	7.2
Steel B[a] (Pipe)		873	997	19.5
Welds[b,c]		908	954	15.2

[a]Average of two tests.
[b]Average of three tests.
[c]Fracture in each tensile specimen occurred in Steel B side of the welds away from the weld centerline.

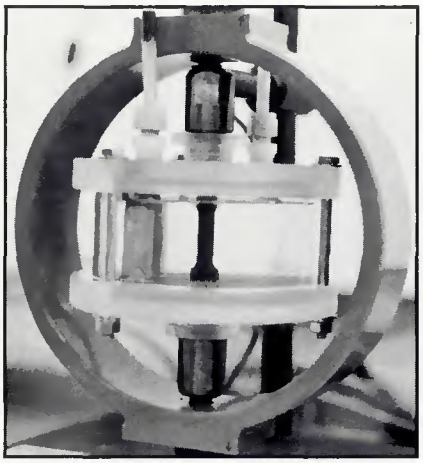

Fig. 1 — The SSC test setup

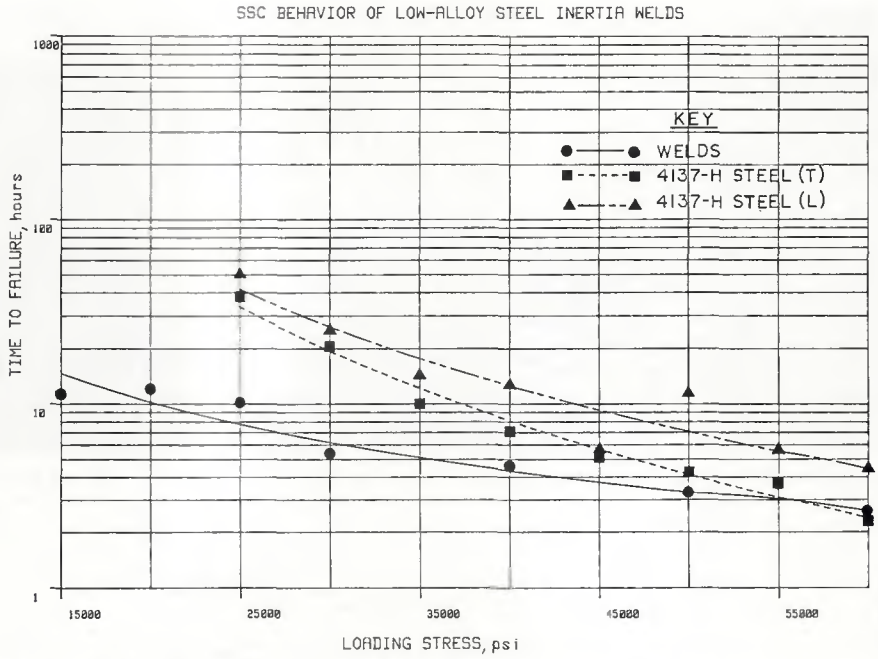

Fig. 2 — Loading stress vs. time to failure plots for the inertia friction welds and AISI 4137-H steel

machine. The fracture surfaces of these specimens contained several shiny areas caused by hydrogen. These surfaces were studied under a scanning electron microscope with an energy dispersive x-ray fluorescence spectrometer. Similarly, two SSC test specimens from AISI 4137-H steel in the transverse direction were loaded in the SSC test cell at 344.7 MPa (50,000 psi) for 3.5 h, unloaded, and fractured in a tensile testing machine. The fracture surfaces of these specimens also exhibited several shiny areas caused by hydrogen that were studied under a scanning electron microscope.

After SSC testing, all the specimens were sectioned longitudinally and examined under an optical microscope. Several microhardness measurements were made at various locations in these specimens near the fracture surfaces.

Results

The SSC Test Results

The loading stress vs. time to failure plots for the inertia friction welds and AISI 4137-H steel in the transverse direction are shown in Fig. 2. Several of the SSC tests were repeated and the shortest observed time to failure was usually used to plot the curves and data points shown in Fig. 2. This was done to take into account the worst cases and compare the performance of the welds and AISI 4137-H steel on a conservative basis.

The curves shown in Fig. 2 are drawn using the linear regression analysis of the data points based on the method of least squares. The standard error of estimate ($S_{y/x}$) values of time to failure (in hours) on loading stress (in psi) for the welds were 1.7 h and 1.8 h for AISI 4137-H steel in the transverse direction. In SSC testing using smooth tensile specimens, the specimens are loaded at different stress levels and the time to failure is monitored in each case. Therefore, time to failure was treated as the dependent variable and plotted on the y-axis and the loading stress was treated as the independent variable and plotted on the x-axis. However, some earlier researchers (Refs. 14, 15) plotted the time to failure on the x-axis and the loading stress on the y-axis.

Since none of the SSC specimens from AISI 4137-H steel in the transverse direction loaded at 137.8 (20,000 psi) broke within 720 h, the plot for AISI 4137-H steel is drawn only up to 172.4 MPa (25,000 psi) and extrapolation of the plot beyond 172.4 MPa (25,000 psi) is not valid. However, the SSC test specimens from the welds were found to be breaking even at stress values as low as 103.4 MPa (15,000 psi). Since the times to failure for SSC test specimens from the welds were very short at high stress levels, specimens were loaded at stress intervals of 34.5 MPa (5000 psi) between loading stress levels of 206.8 MPa (30,000 psi) and 103.4 MPa (15,000 psi) to generate more data points.

From Fig. 2 it is clear that AISI 4137-H steel exhibited superior performance over the welds in the SSC tests. The fact that SSC specimens loaded at 137.8 MPa (20,000 psi) did not break within 720 h clearly shows that AISI 4137-H steel in the transverse direction has better resistance to SSC cracking than the inertia friction welds. The actual time to failure values for the SSC test specimens from AISI 4137-H steel were consistently higher than those for the welds at all stress levels. The low standard error of estimate ($S_{y/x}$) values for both the welds and AISI 4137-H steel indicate that the scatter in the test data is extremely small.

The SEM Study

The SEM study of the SSC specimens from the welds showed several unconnected, flat, shiny areas caused by hydrogen cracking — Fig. 3. Many elongated inclusions were seen all over the fracture surfaces. Several of these elongated inclusions were found at the center of the hydrogen cracks — Fig. 4. The size of the hydrogen cracks varied anywhere from 500 to 3000 μm in diameter.

The predominant mode of fracture in the hydrogen cracks appeared to be quasicleavage, although scattered areas of intergranular separation were found — Fig. 5. The extent of intergranularity varied from one crack to the other. However, SEM study of several of the specimens clearly showed quasicleavage to be the predominant mode of fracture in the hydrogen cracks — Fig. 6. It also appeared that the quasicleavage fracture areas were invariably associated with nonmetallic inclusions. An EDS x-ray analysis of several of the inclusions associated with the hydrogen cracks identified them to be of manganese-iron sulfide type — Fig. 5. Some of these sulfide inclusions seen in the hydrogen cracks were rounded in shape — Fig. 7. The quasicleavage areas exhibited extensive secondary cracking. The quasicleavage fracture areas were joined by microvoid coalescence, which happened to be the fracture mode in the rest of the areas in the specimens — Fig. 8.

The SSC specimens from AISI 4137-H steel in the transverse direction also showed several flat, shiny areas caused by hydrogen cracking — Fig. 9A. The fracture surfaces of these specimens exhib-

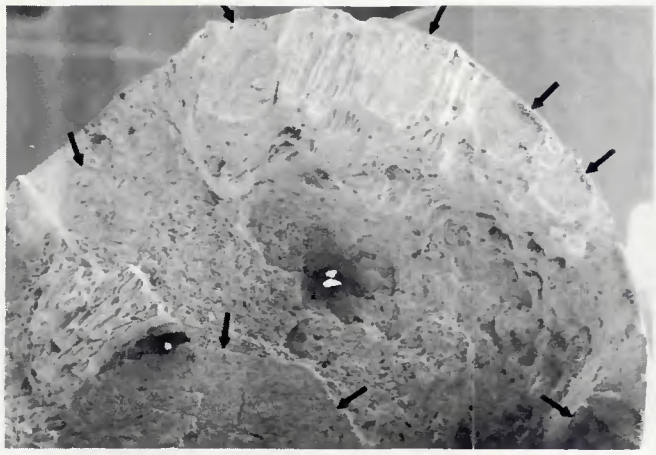

Fig. 3 — Fracture surface of a hydrogen-charged SSC specimen from the welds showing several circular areas of quasicleavage fracture caused by hydrogen. Some of these areas are shown by arrows

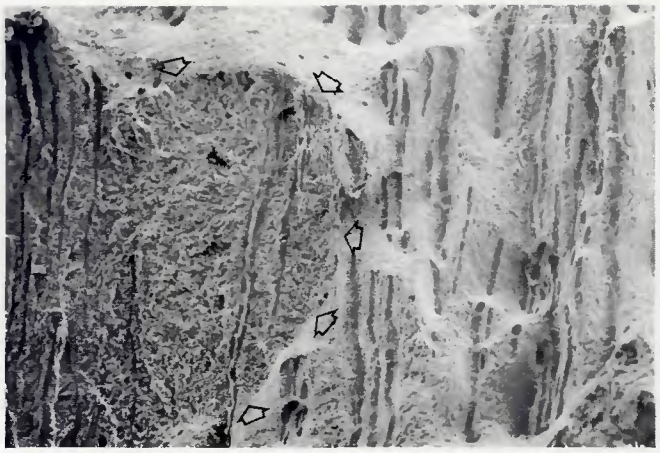

Fig. 4 — SEM view of one of the hydrogen fracture areas (shown by arrows) showing elongated nonmetallic inclusions. Also note the woody appearance of the adjoining areas to the hydrogen crack

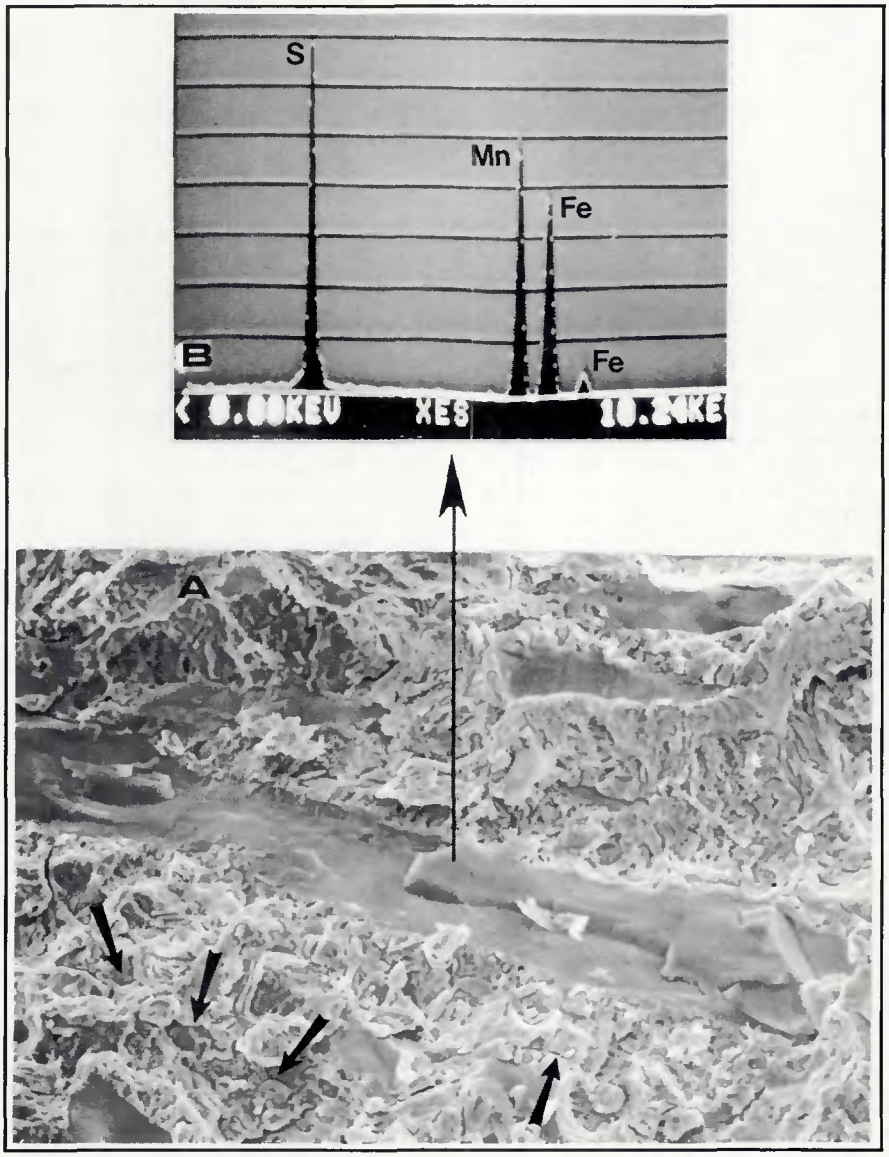

Fig. 5 — A — Hydrogen fracture in the welds showing predominantly quasicleavage fracture mode. Scattered areas of intergranular separation are shown by arrows; B — Energy-dispersive x-ray spectrum from the elongated inclusion seen at the center of Fig. 5 A showing the presence of Mn, Fe and S

ited woody appearance due to the elongated manganese sulfide inclusions. Several of these elongated sulfide inclusions were seen at the center of the hydrogen cracks — Fig. 9B. The predominant mode of fracture in the hydrogen cracks appeared to be by quasicleavage — Fig. 9C. A few scattered, isolated areas of intergranular separation were also faintly noticed in the hydrogen cracks. Extensive secondary cracking was observed in the quasicleavage areas in the specimens — Fig. 9D. Similar to the welds, the quasicleavage areas in these specimens also were joined by microvoid coalescence, which was found to be the mode of fracture in the rest of the areas in the specimens — Fig. 9E.

Apart from the similarities in the fractographic features between the weld (Fig. 3) and AISI 4137-H steel specimens (Fig. 9), some differences were also apparent between them. For example, while the weld specimen showed several small individual hydrogen fracture areas, AISI 4137-H steel specimen showed fewer, but larger, hydrogen fracture areas.

Optical Metallography

Optical metallography of the SSC specimens from the welds revealed that the fracture in many of the specimens occurred very close to the weld centerline between Steel A (AISI 4137-H steel) and Steel B (pipe). In some of the specimens, the fracture appeared to have originated at the weld centerline. However, the propagation of the fracture was found to have occurred only in Steel A — Fig. 10.

Several hydrogen cracks were found to be originating from the elongated manganese sulfide inclusions near the fracture surfaces — Fig. 11. Steel A in the weld area exhibited pronounced banding. Many of the inclusions and the hydrogen cracks were found to be in the dark etching bands — Fig. 12. The Steel B

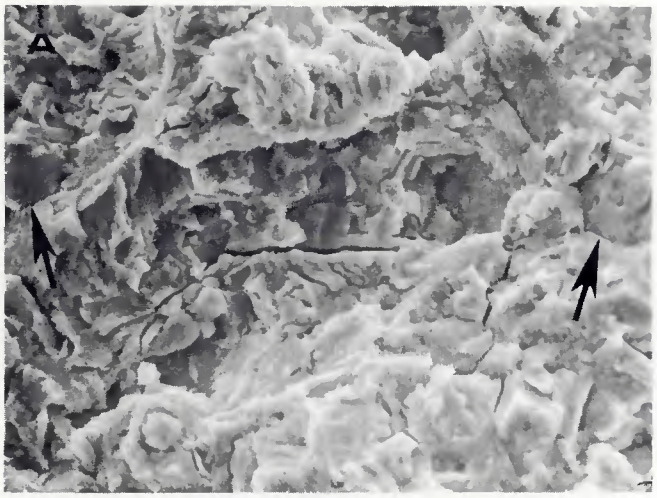

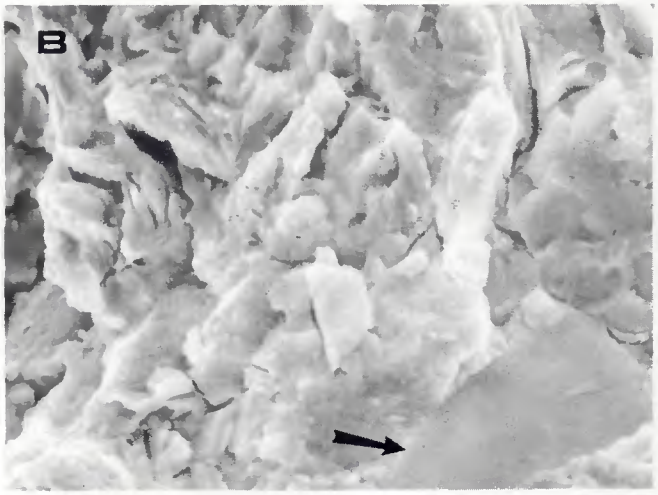

Fig. 6 — Higher magnification views of the quasicleavage fracture morphology in hydrogen fracture areas in the welds. Note the scattered areas of intergranular separation in Fig. 6 A (shown by arrows) and the presence of a sulfide inclusion in Fig. 6 B (shown by an arrow)

side of the welds did not show any such dark and white etching bands.

Although the SSC test specimens from AISI 4137-H steel in the transverse direction did not show any banding at all, the hydrogen cracks were found to be associated with the elongated manganese sulfide inclusions. The direction of propagation of the cracks was perpendicular to the loading axis. A dark film of iron sulfide was noticed on the periphery of many of the specimens. In general, the SSC specimens did not exhibit any pitting attack along the walls.

Discussion

SSC Behavior of the Welds

Due to the reorientation of the grains and inclusions at the weld interfaces as a result of the plastic flow that occurs during inertia friction welding, the elongated nonmetallic inclusions become transversely oriented near the weld centerline with respect to the loading axis — Fig. 13. Such a reorientation of the elongated inclusions appears to drastically increase the susceptibility of the steels to SSC cracking, as can be seen from Fig. 2. This conclusion is supported by the observations that several hydrogen cracks initiated at elongated sulfide inclusions and that the cracks were also associated with these nonmetallic inclusions during the propagation stages.

Since the transverse properties of the inertia friction welds are exposed during the SSC tests, it is not surprising that the welds showed such poor resistance to SSC cracking. However, it is interesting to note that the SSC cracking resistance of the inertia friction welds was inferior to that of AISI 4137-H steel in the transverse direction, where the elongated nonmetallic inclusions are also perpendicular to the loading axis. The explanation for this inferior behavior of the welds can be offered by the microstructural observations made on the SSC specimens from the welds.

The SSC specimens from the welds showed pronounced banding at the weld interface — Fig. 12A. The AISI 4100 series steels are known to exhibit banding of carbon-molybdenum-rich areas in the steels. For example, it was shown through microprobe analysis that a 25.4-mm (1-in.) bar exhibited areas that had carbon content up to 1.5% and molybdenum up to 1%, as opposed to the nominal levels of 0.40% C and 0.20% Mo (Ref. 16). Therefore, when such alloy-rich areas cool to room temperature from forging temperature range (temperature reached near the weld interfaces during inertia friction welding) of the steels, the alloy-rich areas harden (625 VHN) significantly higher than the alloy-lean areas (330 VHN) (Ref. 4). However, when the welds were quenched and tempered, this difference in the hardness between the hard and soft bands was reduced considerably.

Microhardness measurements made

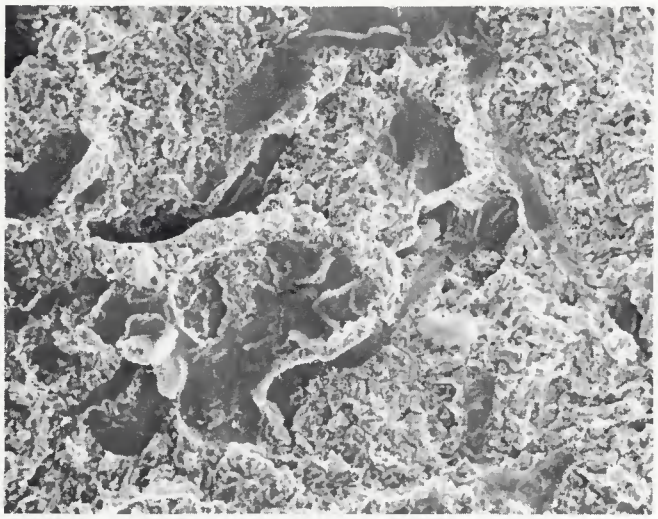

Fig. 7 — Hydrogen fracture area in the SSC specimen from the welds showing rounded sulfide inclusions

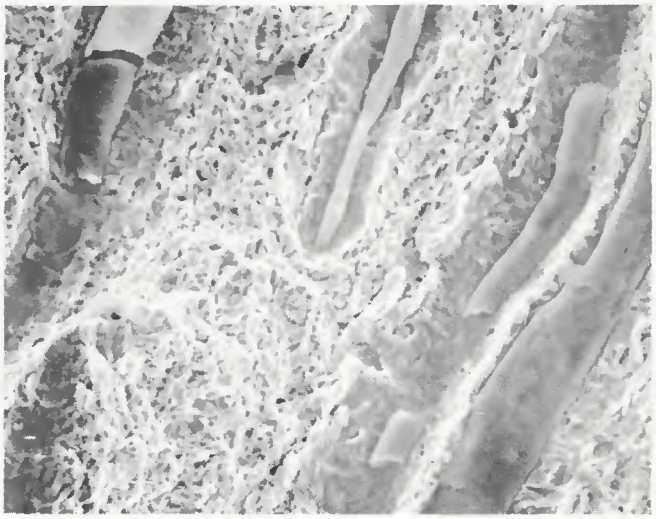

Fig. 8 — SEM view of microvoid coalescence fracture mode in the areas adjoining the hydrogen fracture areas

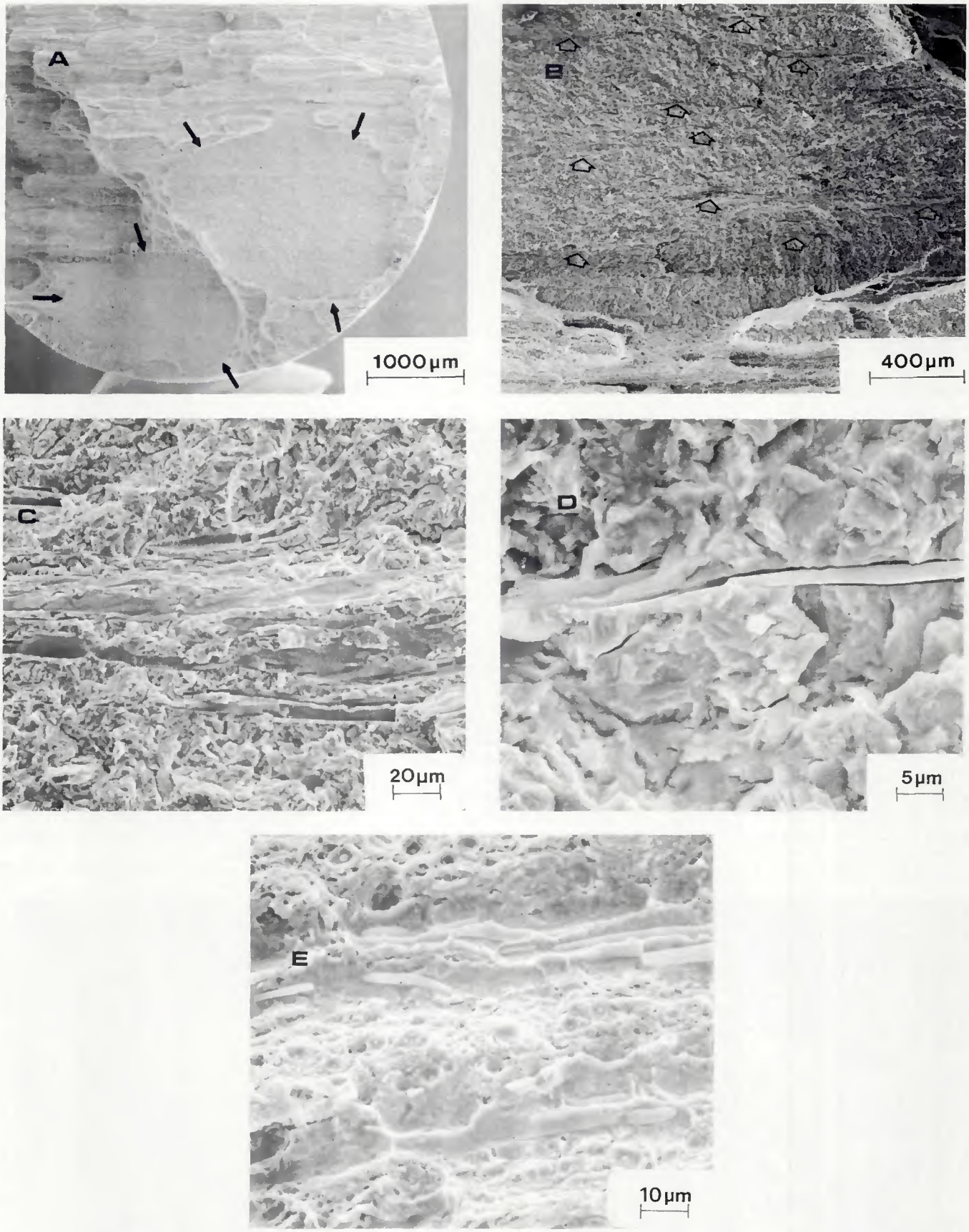

Fig. 9—SEM views of the fracture surfaces of the SSC specimens from AISI 4137-H steel in the transverse direction. A—Overall view showing hydrogen fracture areas (shown by arrows); B—MnS inclusions (shown by arrows) in a hydrogen fracture area; C—Hydrogen fracture area showing quasicleavage fracture morphology; D—Secondary cracking in quasicleavage fracture; E—Microvoid coalescence fracture mode in the areas adjoining hydrogen fracture areas

using 200-g load on Steel A side (AISI 4137-H steel) of the SSC test specimens from the welds indicated the average hardness of the light bands to be 329 VHN (33 HRC), while that of the dark bands was 347 VHN (35 HRC). Hardness values as high as 362 VHN (37 HRC) were obtained on the dark bands. Thus, it is clear that Steel A side of the welds exhibited hard bands.

It was shown earlier by the author that AISI 4137-H steel in the quenched and tempered condition becomes increasingly more susceptible to sulfide stress corrosion cracking as the hardness of the steel is increased (Ref. 12). For example, when the steel was quenched and tempered to a hardness of 30 HRC, the threshold stress below which the specimens did not fail within 720 h in the NACE test was 303 MPa (44,000 psi). When the steel was quenched and tempered to 36 HRC, the same threshold stress dropped to only 110 MPa (16,000 psi). At a hardness of 36 HRC, specimens loaded at 34.5 MPa (5000 psi) in the test cell lasted 720 h without failure. Yet, they exhibited several hydrogen cracks indicating the potentially damaging effect of high hardness on SSC cracking resistance of steels. All these clearly show that the higher the hardness, the more susceptible the steels become to sulfide stress corrosion cracking.

Therefore, it is not surprising that the hydrogen cracks were found in the dark-etching bands that were harder than the light-etching bands. Similar observations were reported in a study on C-75 steel and 90 SS steel tubing that exhibited dark and light etching bands (Ref. 17). Microprobe analysis in these steels showed that the dark etching bands had much higher manganese content than the nominal levels. The hydrogen cracks in both the steels were found in the dark etching bands that were considerably harder than the light etching bands.

Segregation of elements such as carbon, molybdenum and manganese causes the steel to develop higher hardness upon quenching. When such segregated steels are tempered, elements such as molybdenum, chromium and manganese retard softening (Ref. 18). As a result, segregation of alloying elements in steels leads to hard and soft areas after quench and temper treatments.

The average hardness of Steel B in the welds was only 310 HVN (200-g load) (31 HRC). Steel B did not show any banding at all. The high hardness of Steel A compared to Steel B and the presence of banding in Steel A appear to be the reasons why the SSC specimens from the welds failed on Steel A (AISI 4137-H steel) side.

Since the only observed difference between the welds and AISI 4137-H steel in the transverse direction was the presence of banding in Steel A (AISI 4137-H steel) side of the welds, it can be concluded that the presence of banding with hard spots is the reason the SSC cracking resistance of the welds was inferior to that of AISI 4137-H steel in the transverse direction.

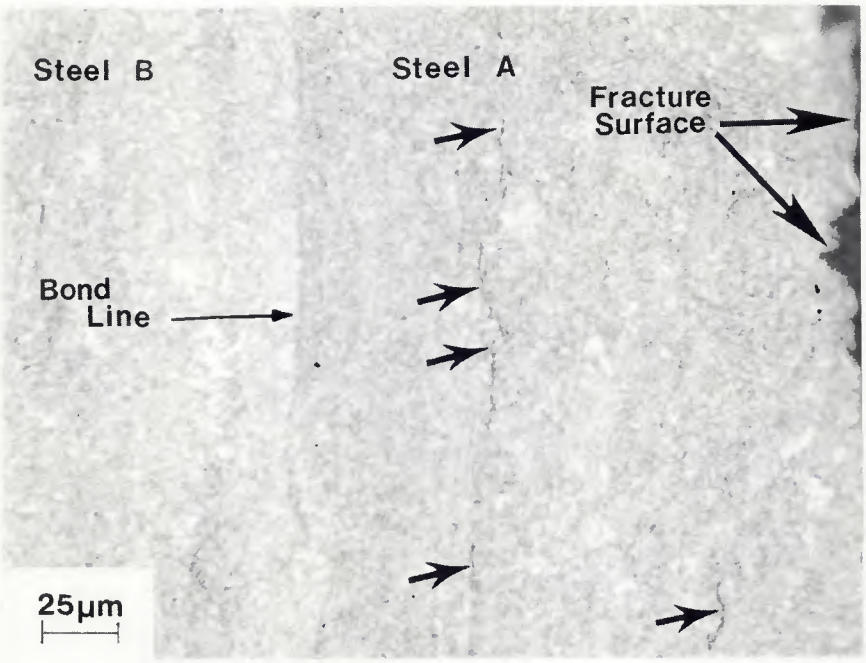

Fig. 10 — Weld area between Steel A and Steel B showing the bond line and the fracture surface. The arrows show some of the inclusion-originated hydrogen cracks. Picral etch

The Effect of Inclusions

Inclusions are known to be good trap sites for hydrogen, and elongated inclusions, in particular, have been known to promote hydrogen embrittlement of steels (Refs. 19, 20). In an earlier study on the SSC cracking behavior conducted at this laboratory on three different heats of

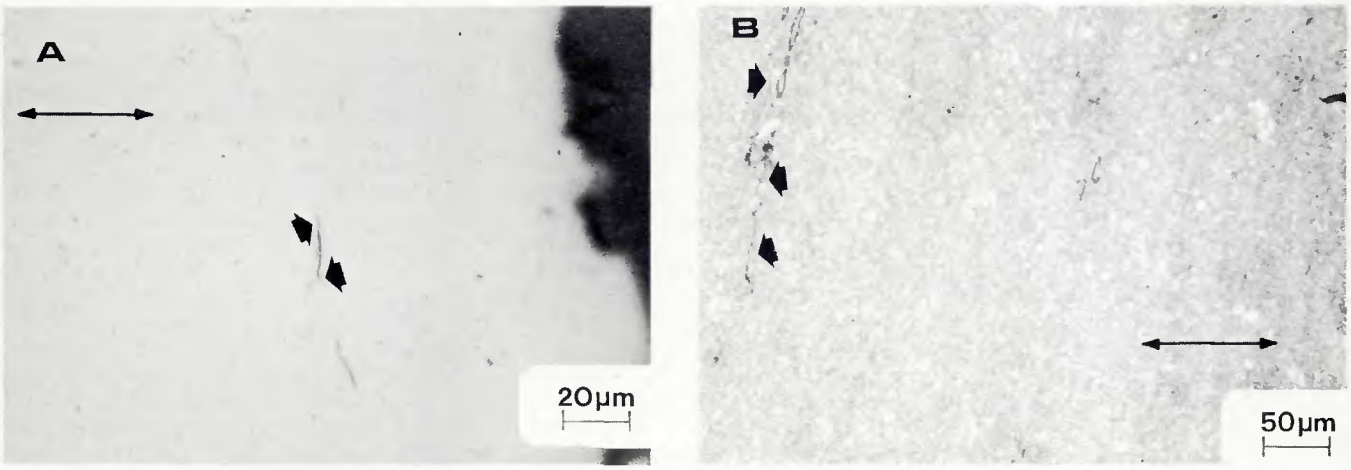

Fig. 11 — View near the fracture surface on Steel A side showing hydrogen cracks (shown by arrows) originating at sulfide inclusions. Horizontal arrows in these figures refer to the loading axis. A — Unetched; B — Etched in picral

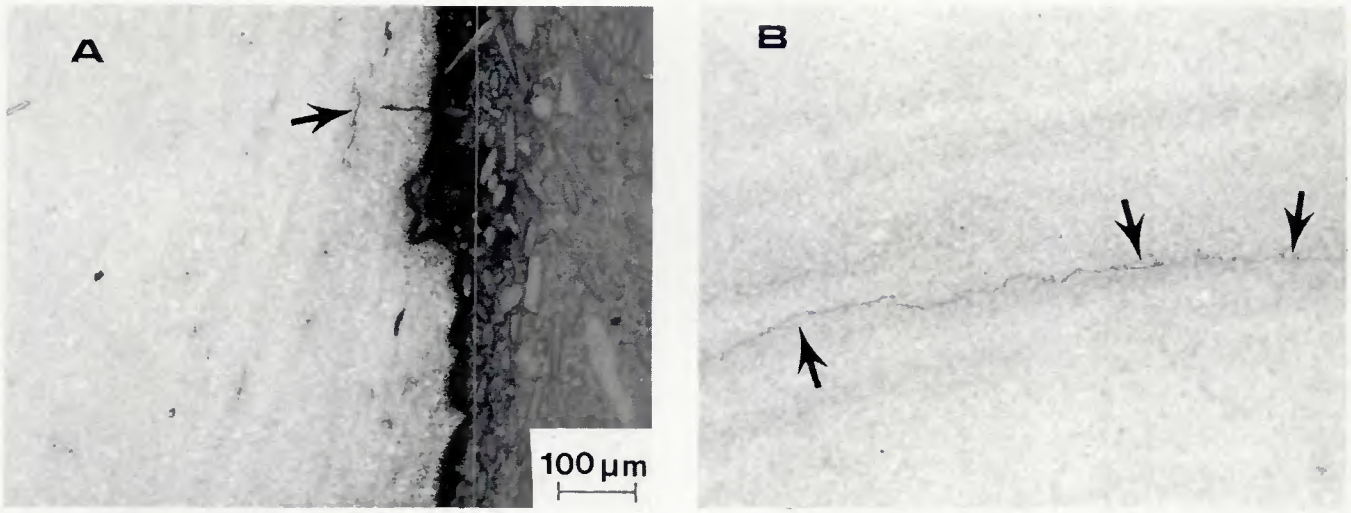

Fig. 12 — Steel A side of the weld near the fracture surface showing hydrogen cracks (shown by arrows) along the dark etching bands. A — Initiation in the dark band; B — Propagation along a dark band

AISI 4137-H steel in the quenched and tempered condition, it was shown that the heat that contained the greatest number of elongated inclusions exhibited the highest susceptibility to SSC cracking (Ref. 21). This study was performed on open-hearth quality (greatest number of elongated inclusions), aircraft quality (in accordance with specification AMS 2301F and with fewest inclusions), and calcium-aluminum deoxidized heats of AISI 4137-H steel. Calcium-aluminum deoxidation was used to globularize the elongated sulfide inclusions. Globularizing the elongated sulfide inclusions was found to improve the SSC resistance of steels over the open-hearth quality heat. The reason for this improvement is that globularizing the elongated inclusions eliminates the notch effect and the stress-induced hydrogen diffusion associated with the elongated inclusions (Ref. 19).

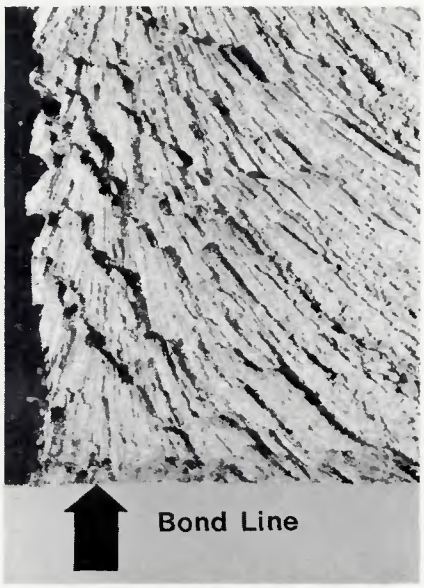

Fig. 13 — Fracture surface of an Izod impact test specimen from the inertia friction weld showing the reorientation of grains at the weld interface

However, it was found that reducing the number of sulfide inclusions by using cleaner grades, as in the aircraft quality heat, was the most effective way to improve the SSC cracking resistance of steels. Similarly, Okhi, *et al.* (Ref. 22), also reported that lowering the sulfur content and controlling the shape of sulfide inclusions by rare-earth additions increased the SSC resistance of C-Mn steels.

In Fig. 2, the SSC cracking behavior of AISI 4137-H steel in the longitudinal direction taken from Ref. 12 is presented for comparison. The SSC specimens taken along the longitudinal axis of the billet were also quenched and tempered at 685°C to a hardness of 33 HRC. The mechanical properties of the steel in the quenched and tempered condition are presented in Table 3 for both the longitudinal and transverse directions.

As can be seen from Table 3, the elongation of the steel in the transverse direction is much lower than that in the longitudinal direction. It is well known that elongated sulfide inclusions drastically reduce the ductility and toughness of steels in the transverse direction (Ref. 23). For example, Izod impact energy values at room temperature for AISI 4137-H steel when quenched and tempered to a hardness of 33 HRC were 84 J (62 ft-lbs) in the longitudinal direction and only 19 J (14 ft-lbs) in the transverse direction.

It is clear from Fig. 2 that the steel exhibited better resistance to SSC cracking in the longitudinal direction than in the transverse direction, as evidenced by the longer times required to cause failure of the specimens at each loading stress level. The only difference between the SSC specimens in the longitudinal and the transverse directions is the orientations of the inclusions with respect to the loading axis. When the SSC specimens are machined along the longitudinal axis of the billet (with respect to the metal working direction) and loaded in the test cell, the elongated sulfide inclusions become parallel to the loading axis. On the other hand, when the SSC specimens are machined along the transverse direction of the billet and loaded, the elongated inclusions become perpendicular to the loading axis.

Therefore, it appears from the results that when the long axis of the elongated inclusions becomes perpendicular to the loading axis, the inclusions become much more effective as stress raisers and initiate cracks readily. This is shown by the fact that several hydrogen cracks were found to have nucleated at the elongated sulfide inclusions and that the times to failure for the SSC specimens taken from the transverse direction were shorter at every loading stress level, compared to those taken from the longitudinal axis.

Hydrogen-induced cracks were found to have initiated in both the welds and AISI 4137-H steel at elongated sulfide inclusions that were oriented transverse to the loading axis. Hydrogen-induced cracks were also found to have initiated at globular manganese sulfide inclusions in AISI 4137-H steel — Fig. 14A. Similarly, it was also observed earlier in a calcium-aluminum deoxidized heat of AISI 4137-H steel that hydrogen cracks originated at globular sulfide inclusions (Ref. 21). These observations further prove that globularizing the elongated sulfide inclusions is only a partial solution to the problem of SSC cracking in low-alloy steels.

Another observation that was made from Fig. 14B is that hydrogen cracks were found to be initiating from and propagating along smaller globular sulfide inclusions (2 μm), while no cracks initiated at a larger inclusion (7 μm). Notice also that the smaller inclusions are spaced

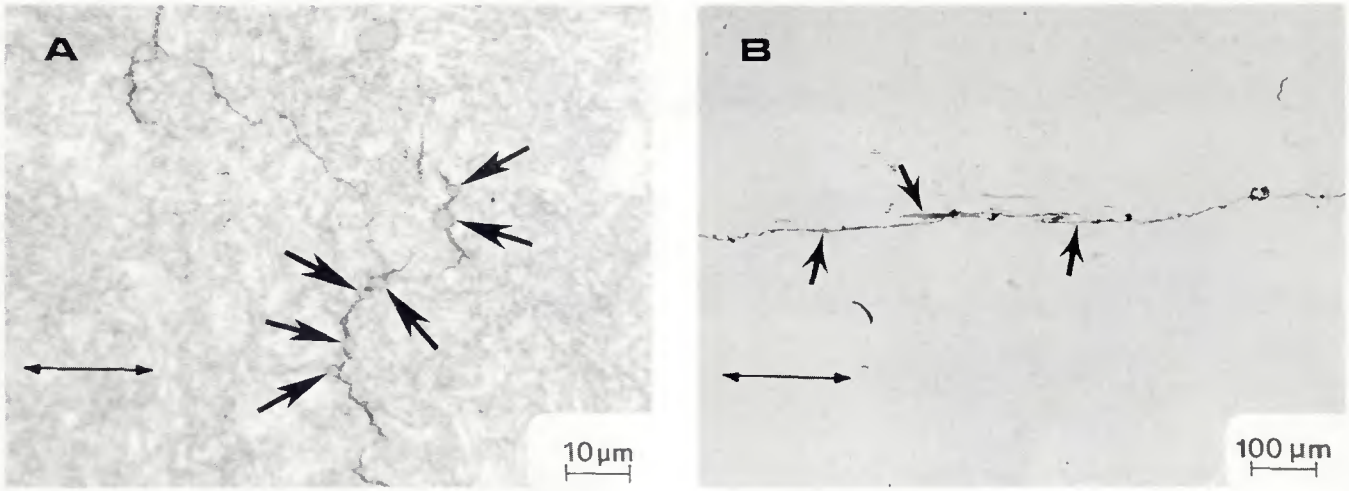

Fig. 14 — Hydrogen cracks originating at globular and elongated manganese sulfide inclusions (shown by arrows). Loading axis in these specimens is shown by the horizontal arrows. Note the direction of propagation of the cracks with respect to the loading axis. A — Transverse specimen; B — Longitudinal specimen

closer, while the larger inclusion is secluded from the rest. Fractographic observations of hydrogen cracks in several heats of AISI 4137-H steel confirmed that, apart from the size of the inclusions, the interinclusion spacing appeared to be equally important in reducing the risk of hydrogen cracking. For example, in an earlier study conducted at this laboratory on the SSC cracking resistance of three different heats of AISI 4137-H steel, the aircraft quality heat (fewest inclusions) performed the best, calcium-aluminum deoxidized heat next best, and the open-hearth quality the worst (Ref. 21). Interinclusion spacing measurements on these heats were 34.5 μm, 27.4 μm and 23.6 μm for aircraft quality heat, calcium-aluminum deoxidized heat and open-hearth quality heat, respectively (Ref. 24). As a result of globularization of the elongated sulfide inclusions from the calcium-aluminum deoxidation, the interinclusion spacing may have increased in this heat.

Therefore, in order to improve the SSC cracking resistance of steels, they should contain as few elongated inclusions as possible and the interinclusion spacing should be as high as possible. This means the use of cleaner steels with fewer inclusions will greatly reduce the risk of SSC cracking in steels.

It is interesting to note in Fig. 14 that the direction of propagation of hydrogen cracks was perpendicular to the loading axis in the transverse specimens and parallel to it in the longitudinal specimens. Although some of the hydrogen cracks traversed along the loading axis in the longitudinal specimens, their directions changed at a later stage and the cracks became perpendicular to the loading axis. However, in the transverse specimens, all the hydrogen cracks observed were transverse to the loading axis. Neither the longitudinal specimens nor the transverse specimens from AISI 4137-H steel showed any banding at all. None of the specimens examined exhibited any noticeable microhardness variations, indicating that, unlike in the welds, there were no hard spots in AISI 4137-H steel specimens that could have guided the cracks along the hard bands.

Some of the longitudinal specimens exhibited hydrogen cracks that originated at specimen side walls, usually from corrosion pits, and propagated transverse to the loading axis. Some internal cracks propagated at 45 deg to the loading axis in the longitudinal specimens. However, a vast majority of the internal hydrogen cracks observed in the longitudinal specimens propagated along the longitudinal direction of the billet. Therefore, it appeared from these observations that, for reasons not clear, the hydrogen cracks exhibited a tendency to propagate along the longitudinal direction (with respect to the metalworking direction) of the billet.

Interrupted SSC Tests

The SEM observation of the fracture surfaces of the SSC test specimens that broke in the test cell showed that they were covered by a black film. An EDS x-ray analysis revealed that the film consisted of Fe and S. The iron sulfide film results from the interaction between H_2S and the steel. Since the iron sulfide film impedes the understanding of the fracture mode, and therefore, the mechanism of failures, Interrante and Hicho tried several methods to remove the tenacious film of FeS (Ref. 25). They found that hydrogen reduction of the sulfide film at elevated temperatures yielded the best results. Caution had to be exercised while using this procedure, since exposure of the sulfide film to hydrogen at elevated temperature resulted in the formation of H_2S gas.

Several solutions were tried at this laboratory to remove the FeS film from the fracture surfaces of the SSC test specimens that broke in the test cell (Ref. 12). Although some of the solutions removed the tenacious FeS film from the fracture surfaces, they were found to attack the base metal, hence considered unsatisfactory. It was then that the author conceived the idea of interrupted tests to produce the hydrogen fracture areas in the test specimens.

The philosophy of the interrupted tests is explained in detail in Ref. 12. Briefly, it was found through optical metallography that many unbroken specimens that survived 720 h in the NACE test exhibited numerous hydrogen cracks. Some of these cracks were quite long and not open to the surface. Therefore, if a SSC specimen in which many hydrogen cracks initiated is unloaded from the SSC test cell before fracture and then pulled in a tensile testing machine to failure, it should be possible to have clean hydrogen fracture surfaces that are not covered by FeS film. This would then eliminate the need for any cleaning of the fracture surfaces prior to the SEM study.

Accordingly, several replicate specimens from the welds and AISI 4137-H steel in the transverse direction were loaded in the test cell. Since predicted times to failure were established in Fig. 2, these replicate specimens were unloaded from the SSC test cell before failure and later fractured in a tensile testing machine. The fracture surfaces of these replicate specimens contained several clean hydrogen fracture areas — Figs. 3 and 9A. Since the replicate specimens were fractured outside the test cell, the problem of the formation of tenacious black film of iron sulfide on the fracture surfaces was eliminated. The absence of FeS film on the fracture surfaces also

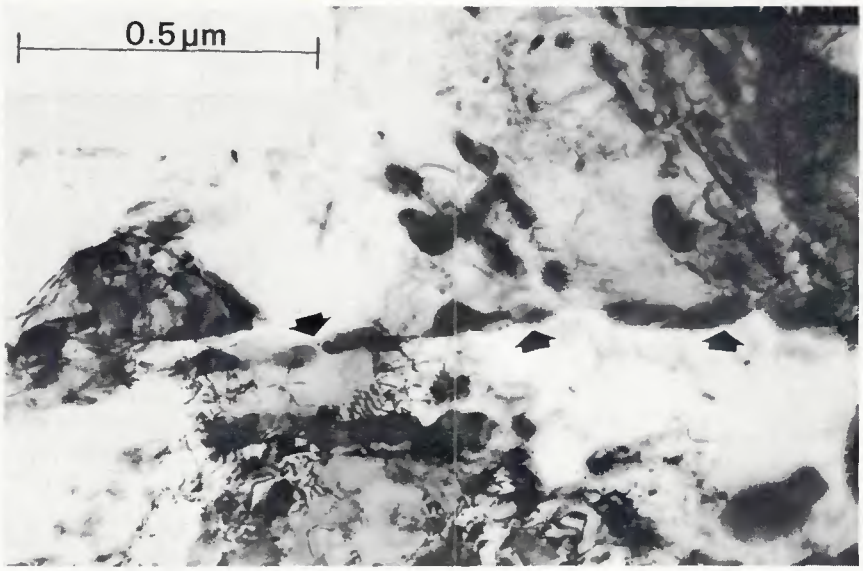

Fig. 15 — TEM photograph showing the substructure of the specimens from AISI 4137-H steel tempered at 565°C. Notice the grain boundary precipitation of needle-like carbides (shown by arrows) (after Ref. 12)

establishes that the cause of embrittlement in the SSC tests is hydrogen, and not hydrogen sulfide.

Since these replicate specimens were loaded for a few hours and unloaded from the SSC test cell, they were referred to as "interrupted test specimens." Comparison of the hydrogen fracture morphologies in the interrupted test specimens with the actual SSC test specimen that broke in the test cell showed that they were identical (Ref. 12). Therefore, the method of producing hydrogen fracture areas in the SSC test specimens by interrupting the SSC test before the specimens fail and later fracturing them in a tensile testing machine was found to be excellent for studying hydrogen fracture morphologies in laboratory SSC tests using smooth tensile specimens.

When the replicate specimens were interrupted from the SSC test and fractured in a tensile testing machine to produce hydrogen fracture areas, all of them broke at considerably lower stress values than their tensile strength. For example, some specimens broke at stress values as low as 537 MPa (78,000 psi). This is because exposure of these replicate specimens to H_2S in the test cell initiated several hydrogen cracks in them (as revealed later by the SEM study). However, the most important observation made during the tensile testing of interrupted SSC specimens was that the elongation in the hydrogen-charged specimens dropped drastically. The elongation in the hydrogen-charged SSC specimens from the welds was only around 2.5%, whereas the average elongation in the tensile specimens from the welds was 15.2% (from Table 3).

Therefore, it is evident that exposure of the SSC specimens to hydrogen sulfide had severely embrittled them. This embrittling effect of hydrogen sulfide is also evident from the fact that two SSC specimens from the welds stressed at 137.9 MPa (20,000 psi) and 344.7 MPa (50,000 psi) survived in the cell for 300 h without failure in the absence of hydrogen sulfide. However, two more SSC specimens from the welds loaded in the test cell at the same stress values when exposed to hydrogen sulfide failed in 12.0 h and 3.3 h, respectively.

Accompanying this embrittlement was the change in the fracture morphology observed in the specimens. The hydrogen fracture areas showed quasicleavage fracture with scattered areas of intergranular separation, whereas the rest of the areas in both the welds and AISI 4137-H steel showed ductile fracture involving microvoid coalescence.

Hydrogen Fracture Morphology

The presence of predominantly transgranular quasicleavage fracture mode with scattered areas of intergranular separation in the welds and AISI 4137-H steel is consistent with the earlier findings reported on this steel when it was quenched and tempered to 33 HRC (Refs. 12, 21). It is interesting to note that the same steel when quenched and tempered to 33 HRC at 685°C (1265°F) and 565°C (1049°F) exhibited different fracture morphologies. Tempering the steel to 33 HRC at 685°C showed a predominantly quasicleavage fracture morphology with scattered areas of intergranular separation. When the same steel was tempered at 565°C to 33 HRC, the fracture morphology consisted of both intergranular separation and quasicleavage mode, indicating an increase in the extent of intergranularity (Ref. 12). The 565°C temper also lowered the SSC resistance of the steel, compared to 685°C temper.

The transmission electron microscope (TEM) study of the specimens showed that 565°C temper caused the precipitation of needle-like carbides along the prior austenite grain boundaries (Fig. 15), a phenomena that was absent in the specimens tempered at 685°C. The carbides were more uniformly distributed and exhibited a higher degree of spheroidization on 685°C temper, compared to 565°C temper.

Precipitation of needle-like carbides along the prior austenite grain boundaries and the segregation of phosphorus to the grain boundaries were found to accelerate the crack propagation due to SSC in steels (Ref. 26). Studying the effect of impurities and hydrogen on the intergranular fracture of 4340 type steels, Banerji, *et al.* (Ref. 27), found evidence of phosphorus and carbon in excess on the intergranular surfaces. They argued that grain boundary carbide platelets can act as effective barriers to dislocations. A dislocation pile-up can, therefore, cause fracture along the prior austenite grain boundaries that are already weakened by impurity segregation. Therefore, in order to improve the resistance of steels to SSC (and hence hydrogen-induced) cracking, the heat treating variables should be selected so as to avoid precipitation of needle-like carbides along the prior austentite grain boundaries.

The cleanliness of the steels was also found to have a profound effect on their hydrogen fracture morphology, even when the steels received similar heat treatments. For example, aircraft quality heat of AISI 4137-H steel quenched and tempered at 685°C to 33 HRC showed only quasicleavage fracture mode, whereas an open-hearth quality heat of the same steel showed intergranular areas scattered in the quasicleavage areas (Ref. 21). The only difference between the two heats was in the levels of sulfur and phosphorus. The aircraft quality heat had lower levels of these two elements compared to the open-hearth quality heat.

It is well established that hydrogen-induced intergranular fracture is promoted by the segregation of phosphorus and sulfur at the prior austenite grain boundaries (Refs. 26–33). Takeda and McMahon (Ref. 34) were able to produce both transgranular and intergranular cracking in specimens from 5% Ni steel (based on HY130) with virtually identical microstructure and strength, but minor differences in composition. The specimens in their study were quenched and tempered to a hardness of 34.5 ± 1.5 HRC (yield strength of 1060 MPa/154 ksi). They concluded that the stress-controlled intergranular cracking is due to

the segregation of impurities (cohesion lowering elements) to the grain boundaries during making, processing or aging of steel, whereas the strain-controlled quasicleavage mode (also referred to as plasticity-related hydrogen-induced cracking) is intrinsic to steels.

The strength level of the steel was also found to have a profound effect on the hydrogen fracture morphology of quenched and tempered low-alloy steels. It was shown that the steels exhibited increasingly more intergranular fracture as their strength (and therefore hardness) was increased (Refs. 12, 28, 32). This is because as the strength level of the steel is increased, it becomes increasingly more sensitive to the presence of even minute quantities of impurities. For example, it was shown that at high yield strengths (1516 MPa/220 ksi) even 50 ppm of phosphorus (bulk concentration) was found to be sufficient to cause intergranular separation in 4130 type steels (Ref. 35).

Therefore, it is clear from the results of Takeda and McMahon (Ref. 34) and those of this author (Refs. 12, 21) that whether a particular type of steel will exhibit transgranular or intergranular cracking due to hydrogen will depend on the strength level of the steel, the heat treatment it received, the amount of impurities present in the steel, and the ability of these impurities to segregate to the grain boundaries in the steel. Therefore, in view of all these variables that can affect the hydrogen fracture morphology in quenched and tempered low-alloy steels, one has to be careful in judging the significance of the fractographic results obtained.

It appeared from the SEM examination of the hydrogen cracks that the cracks were following the boundaries between martensite laths—Fig. 16. The quasicleavage fracture caused by hydrogen is thought to consist of glide plane decohesion in martensite laths and interface decohesion between laths (Ref. 34). The TEM examination of thin foils from AISI 4137-H steel tempered at 685°C showed the presence of needle-like carbides along martensite lath boundaries and smaller, more spheroidized carbides within the laths (Ref. 12). Therefore, cracking along the interlath carbides can be considered to be occurring along the subgrain boundaries, caused by tempering and cracking along intralath carbides through the subgrains. Similarly, Craig and Krauss (Ref. 28) also found the two types of fractures (*viz.*, along the subgrain boundaries and through the subgrains) occurring in the transgranular cracking caused by hydrogen in 4130 type steels.

Since the growth of the quasicleavage areas caused by hydrogen was stopped in the interrupted SSC test specimens, they remained as individual areas. When these interrupted SSC specimens were later fractured in a tensile testing machine, the quasicleavage areas were joined by ductile fracture involving microvoid coalescence.

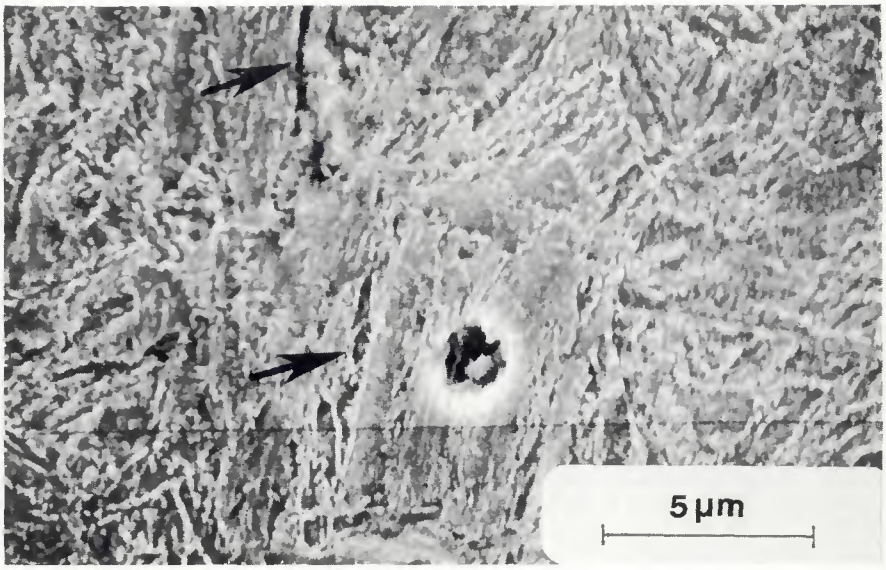

Fig. 16—SEM view of the hydrogen crack tip in the SSC specimens. The small white particle in the pit was found to be an alumina inclusion. Picral etch

The quasicleavage areas caused by hydrogen were found to have invariably originated from inclusions. In the present study, many of these inclusions have been identified to be manganese and iron sulfide types. The hydrogen cracks were also found to have initiated at alumina, silica and titanium nitride inclusions (Refs. 17, 21, 28, 36, 37). This is because these inclusions can act as hydrogen sinks and can act as sources of hydrogen when the steels are stressed. Giuliani, *et al.* (Ref. 37), explained the embrittlement process as the activation and inactivation of hydrogen-collecting traps, where the trap was assumed as the zone of high triaxial stresses at the tip of an inclusion-containing cavity.

Conclusions

Based on the SSC cracking study of quenched and tempered low-alloy steel inertia friction welds and AISI 4137-H steel in the transverse direction, the following conclusions may be drawn:

1. The SSC cracking resistance of AISI 4137-H steel in the transverse direction was inferior to that of the same steel in the longitudinal direction (with respect to the metalworking direction), as evidenced by the shorter times to failure for the transverse specimens at each loading stress level.

2. The presence of several elongated sulfide inclusions in the hydrogen crack surfaces and the fact that several hydrogen cracks initiated from the elongated inclusions that are oriented transversely to the loading axis suggest that the elongated sulfides are the primary sites for crack initiation in H_2S environments.

3. The shorter times to failure exhibby the transverse specimens, compared to the longitudinal specimens, show that the elongated inclusions become much more effective as stress raisers and initiate cracks readily when their long axis is perpendicular to the loading axis.

4. The fact that cracks were found to be initiating at and propagating through globular sulfide inclusions shows that globularizing the elongated sulfide inclusions is not a total solution to the problem of SSC cracking.

5. The SSC cracking resistance of quenched and tempered inertia friction welds between AISI 4137-H steel and Grade E pipe (per API specification 5A) was very poor compared to that of AISI 4137-H steel in the transverse direction. This poor SSC cracking resistance of the inertia friction welds is attributed to the presence of banding in AISI 4137-H steel near the weld interfaces. The hydrogen cracks were found to be propagating along the dark bands that were harder than the nominal hardness of the steel. The banding caused by the segregation of alloying elements (such as manganese, molybdenum, etc.) results from the plastic flow during inertia friction welding.

6. All the welds broke on the Steel A (AISI 4137-H) side in the SSC tests. This was found to be due both to the higher hardness of this steel compared to Steel B (API Grade E pipe), and the presence of banding in it.

7. The absence of FeS film on the fracture surfaces in the interrupted SSC test specimens shows that the cause of embrittlement in hydrogen sulfide environments is hydrogen and not hydrogen sulfide.

References

1. Troiano, A. R., and Hehemann, R. F. 1982. Hydrogen embrittlement and stress corrosion cracking in sour environments. *Current Solutions to Hydrogen Problems in Steel,* Proc. of the First Int'l. Conf., Ed. C. G. Interrante and G. M. Pressouyre, ASM, Metals Park, Ohio, pp. 299–302.

2. Berkowitz, B. J., and Heubaum, H. May 1984. The role of hydrogen in sulfide stress cracking of low alloy steels *Corrosion* 40(5):240–245.

3. Snape, E. 1981. Role of composition and microstructure in sulfide cracking of steel. *H_2S Corrosion in Oil and Gas Production—A Compilation of Classic Papers,* Eds. R. N. Tuttle and R. D. Kane, NACE, Houston, Tex., pp. 108–129.

4. Tumuluru, M. D. 1984. A parametric study of inertia friction welding for low alloy steel pipes. *Welding Journal* 63(9):289-s to 294-s.

5. Grobner, P. J., Sponseller, D. L., and Cias, W. W. June 1975. Development of high strength H_2S resistant steels for oil field applications. *Materials Performance,* pp. 35–43.

6. Mauzy, H. L. 1980. Tool joints for sour drilling environments. *Materials Performance* 19(10):23.

7. Straatmann, J. A., and Smith, Y. E. 1981. Quenched and tempered oil country tubular goods provide improved performance properties for hostile oil and gas drilling environments. *H_2S Corrosion in Oil & Gas Production—A Compilation of Classic Papers,* Eds. R. N. Tuttle and R. D. Kane, NACE, Houston, Tex., pp. 572–578.

8. Sponseller, D. L., Garber, R., and Cox, T. B. 1982. Design of H_2S resistant steels for tubular products used in oil and gas wells. *Current Solutions to Hydrogen Problems in Steel,* Proc. of the First Int'l. Conf., Eds. C. G. Interrante and G. M. Pressouyre, ASM, Metals Park, Ohio, pp. 515–524.

9. Garber, R. 1983. High hardenability low alloy steels for H_2S resistant oil country tubulars. *Corrosion* 39(3):83–91.

10. Lippold, J. C., and Odegard, 8. C. 1984. Technical note: microstructural evolution during inertia friction welding of austenitic stainless steels. *Welding Journal* 63(1):35-s to 38-s.

11. Eberhard, B. J., Schaff, Jr., B. W., and Wilson, A. D. 1983. Friction weld ductility and toughness as influenced by inclusion morphology. *Welding Journal* 62(7):171-s to 178-s.

12. Tumuluru, M. D. 1985. Sulfide stress corrosion cracking of quenched and tempered AISI 4137-H steel. *Materials Performance* 24(7):38–43.

13. *Testing of Metals for Resistance to Sulfide Stress Cracking at Ambient Temperatures.* 1977. NACE Standard TM-01-77, NACE, Houston, Tex.

14. Burns, D. S. January 1976. Laboratory tests for evaluating alloys for H_2S service. *Materials Performance,* pp. 21–27.

15. Greer, J. B. September 1972. Results of interlaboratory sulfide stress cracking using the NACE T-IF-9 proposed test method. *Materials Performance,* pp. 9–15.

16. Kern, R. F., and Suess, M. E. 1978. *Steel Selection—A Guide for Improving Performance and Profits.* John Wiley & Sons, New York, N.Y., p. 78.

17. Ciaraldi, S. W. 1984. Microstructural observations on the sulfide stress cracking of low alloy steel tubulars. *Corrosion* 40(2):77–81.

18. Grange, R. A., Hribal, C. R., and Porter, L. F. 1977. Hardness of tempered martensite in carbon and low alloy steels. *Met. Trans. A,* Vol. 8A, pp. 1775–1785.

19. Pressouyre, G. M. 1982. *Current Solutions to Hydrogen Problems in Steel,* Proc. of the First Int'l. Conference, Eds. C. G. Interrante and G. M. Pressouyre, ASM, Metals Park, Ohio, pp. 18–36.

20. Savage, W. F., Nippes, E. F., and Szekeres, E. S. 1976. Hydrogen induced cold cracking in a low alloy steel. *Welding Journal* 55(9):276-s to 283-s.

21. Tumuluru, M. D. The effects of steel cleanliness and inclusions on the sulfide stress corrosion cracking of AISI 4137-H steel. *Corrosion* 41(7):406–414.

22. Okhi, T., *et al.* 1976. *Stress Corrosion—New Approaches,* Ed. H. L. Craig, Jr., STP 610, ASTM, Philadelphia, Pa., pp. 399–419.

23. Spitzig, W. A. 1983. Effect of sulfides and sulfide morphology on anisotropy of tensile ductility and toughness of hot rolled C-Mn steels. *Met. Trans. A,* Vol. 14A, 471–484.

24. Tumuluru, M. D. Wear resistance of quenched and tempered AISI 4137-H steel. *Met. Trans. A,* Vol. 17A, pp. 295–306.

25. Interrante, C. G., and Hicho, G. E. 1976. *Stress Corrosion—New Approaches,* Ed. H. L. Craig, Jr., STP 610, ASTM, Philadelphia, Pa., pp. 349–365.

26. Morikawa, H., Murata, T., and Inoue, T. 1982. *Current Solutions to Hydrogen Problems in Steels,* Proc. of the First Int'l. Conference, Eds. C. G. Interrante and G. M. Pressouyre, ASM, Metals Park, Ohio, pp. 219–224.

27. Banerji, S. K., McMahon, Jr., C. J., and Feng, H. D. February 1978. Intergranular fracture in 4340-type steels: effects of impurities and hydrogen. *Met. Trans. A,* Vol. 9A, pp. 237–247.

28. Craig, B. D., and Krauss, G. November 1980. The structure of tempered martensite and its susceptibility to hydrogen stress cracking. *Met. Trans. A,* Vol. 11A, pp. 1799–1807.

29. Materkowski, J. P., and Krauss, G. November 1979. Tempered martensite embrittlement in SAE 4340 steel. *Met. Trans. A,* Vol. 10A, pp. 1643–1651.

30. Sponseller, D. L., Garber, R., and Straatman, J. A. 1983. *Optimization of Processing, and Service through Microstructural Control,* Eds. Abrams, Clark, Hood, and Seth, STP 792, ASTM, Philadelphia, Pa., pp. 172–204.

31. Costa, J. E., and Thompson, A. W. May 1981. Effect of hydrogen on fracture behavior of a quenched and tempered medium-carbon steel. *Met. Trans. A,* Vol. 12A, pp. 761–771.

32. Bandyophdhyay, N., Kameda, J., and McMahon, Jr., C. J. May 1983. Hydrogen induced cracking in 4340-type steel: effects of composition, yield strength, and H_2 pressure. *Met. Trans. A,* Vol. 14A, pp. 881–888.

33. McMahon, Jr., C. J. 1981. *Hydrogen Effects in Metals,* Eds. I. M. Bernstein and A. W. Thompson. The Metallurgical Society of AIME, Warrendale, Pa., pp. 219–233.

34. Takeda, Y., and McMahon, Jr., C. J. July 1981. Strain controlled vs. stress controlled hydrogen induced fracture in a quenched and tempered steel. *Met. Trans. A,* Vol 12A, pp. 1255–1266.

35. Craig, B. D. May 1982. The effect of phosphorus content on the hydrogen stress cracking of high strength 4130 steel. *Met. Trans. A,* Vol. 13A, pp. 907–912.

36. Cialone, H., and Asaro, R. J. 1981. Hydrogen effects in the fracture of spheroidized plain carbon steels. *Hydrogen Effects in Metals,* Eds. I. M. Bernstein, and A. W. Thompson, The Metallurgical Society of AIME, Warrendale, Pa., pp. 767–776.

37. Giuliani, L., Mirabile, M., and Sarracino, M. 1974. Embrittlement kinetics of N-80 steel in H_2S environment. *Met. Trans. A,* Vol. 5, pp. 2069–2073.

WRC Bulletin 315
June 1986

Stress Rupture Behavior of Postweld Heat Treated 2¼ Cr-1Mo Steel Weld Metal
By C. D. Lundin, S. C. Kelley, R. Menon and B. J. Kruse

WRC Bulletin 315 complements Bulletin 277, issued in May 1982. Together, these bulletins address the creep properties of 2¼Cr-1Mo steel weld metal deposited with several different welding processes. They contain data obtained from the literature as well as from the many tests conducted on this program. The experimental data, in both reports, are for weld metal of several different carbon contents, postweld heat treated at either of two commonly used postweld heat treating temperatures.

Publication of this report was sponsored by the Subcommittee on Weld Metals and Welding Procedures of the Pressure Vessel Research Committee of the Welding Research Council. The price of WRC Bulletin 315 is $18.00 per copy, plus $5.00 for postage and handling. Orders should be sent with payment to the Welding Research Council, Ste. 1301, 345 E. 47th St., New York, NY 10017.